Quantum simulation of dissociative ionization of H_2^+ in full dimensionality with a time-dependent surface-flux method

Jinzhen Zhu [*]

Physics Department, Ludwig Maximilians Universität, D-80333 Munich, Germany

The dissociative ionization of H_2^+ in a linearly polarized, 400-nm laser pulse is simulated by solving a three-particle time-dependent Schrödinger equation in full dimensionality without using any data from quantum chemistry computation. The joint energy spectrum (JES) is computed using a time-dependent surface-flux method, the details of which are given. The calculated ground energy is -0.597 atomic units and the internuclear distance is 1.997 atomic units if the kinetic energy term of protons is excluded, consistent with the reported precise values from quantum chemistry computation. If the kinetic term of the protons is included, the ground energy is -0.592 atomic units with an internuclear distance of 2.05 atomic units. Energy sharing is observed in JES and we find the peak of the JES with respect to the nuclear kinetic energy release is within 2–4 eV, which is different from previous two-dimensional computations (over 10 eV), but is close to the reported experimental values. The projected energy distribution on the azimuth angles shows that the electron and the protons tend to dissociate in the direction of polarization of the laser pulse.

I. INTRODUCTION

Understanding the three-body Coulomb interaction problem is an ongoing challenge in attosecond physics. The typical candidates for investigation include the helium atom and H_2^+ molecule. In attosecond experiments, a short, intense laser pulse is introduced as a probe for the measurements. Various mechanisms were proposed in recent decades to describe the dissociation and dissociative ionization of H_2^+, including bond softening [1], charge-resonance-enhanced ionization (CREI) [2], bond hardening [3], above threshold dissociation (ATD) [4,5], high-order-harmonic generation (HHG) [6], and above threshold explosion [7]. One may find a summary of the above mechanisms in theoretical and experimental investigations of H_2^+ in the literature [8,9]. Experimental studies on the H_2^+ ion exposed to circular and linearly polarized pulses for angular and energy distributions of electrons were reported recently [10–13].

In theory, the joint energy spectra (JES) of the kinetic energy release (KER) for one electron and two protons of the H_2^+ ion are predominant observables that show how energy distributes around the fragments, where the JES is represented by the KER of two electrons for double ionization (DI) [14–16]. In theory, JES computations for double ionization in full dimensionality were very scarce for laser pulses with wavelengths beyond the XUV regime ($\geqslant 400$ nm) because the computational consumption scales dramatically with the wavelength and intensity of the laser field [16]. With the time-dependent surface-flux (t-SURFF) method, which was first introduced in Ref. [17], a full dimensional simulation of the JES for double ionization was available with moderate computational resources for 800-nm [16] and 400-nm [18] laser pulses. The t-SURFF method was also successfully ap-

plied to the dissociative ionization of the H_2^+ ion [19,20] in a two-dimensional (2D) model, where the energy sharing of the photons and electron is observed in JES.

The dissociative ionization of the H_2^+ ion has been simulated by many groups [10,14,21–26]. However, they are all in reduced dimensionality. Quantum simulation in full dimensionality is not yet available. Although the correlation among the fragments could be observed in the 2D model, the peaks of the JES with total nuclear KER are always above 10 eV. This is far from the experimental observables [11–13], which are usually below 5 eV. The tRecX code, which successfully implements the t-SURFF method in full dimensionality, has been applied successfully in the simulations of the double ionization of helium [16] and the single ionization of polyelectron molecules [27–31]. The dissociative ionization of the H_2^+ ion has not been computed using the tRecX code from before, even in reduced dimensionality.

In this paper, we will introduce simulations of the dissociative ionization of the H_2^+ ion by solving the time-dependent Schrödinger equation (TDSE) in full dimensionality based on the tRecX code. We will first present the computational method for scattering amplitudes with t-SURFF methods, from which the JES can be obtained. Then we will introduce the specific numerical recipes for the H_2^+ ion based on the existing discretization methods of the tRecX code. With such numerical implementations, the *ab initio* calculation of the field-free ground energy of the Hamiltonian is available. Finally, we will present results of dissociative ionization in a 400-nm laser pulse, the JES, and projected energy spectrum on the azimuth angle.

II. METHODS

In this paper, atomic units with $\hbar = e^2 = m_e = 4\pi\epsilon_0 \equiv 1$ are used if not specified. The center of the mass of two protons

―――――――
*Jinzhen.Zhu@physik.uni-muenchen.de

is chosen to be the origin. Instead of using the vector between two protons $\vec{R}$ as a coordinate [14,19,20], we specify the coordinates of the protons and electrons as $\vec{r}_1$, $-\vec{r}_1$, and $\vec{r}_2$. We denote $M = 1836$ atomic units as the mass of the proton.

A. Hamiltonian

The total Hamiltonian can be represented by the sum of the electron-proton interaction H_{EP} and two tensor products, written as

$$H = H_B = H^{(+)} \otimes \mathbb{1} + \mathbb{1} \otimes H^{(-)} + H_{EP}, \quad (1)$$

where the tensor products are formed by the identity operator $\mathbb{1}$ multiplied by the Hamiltonian for two protons ($H^{(+)}$), or that for the electron ($H^{(-)}$). H_B is called the Hamiltonian in the B region and will be detailed later. With the coordinate transformation used in Ref. [32], which is also illustrated in Appendix A for our specific case, the single operator for the electron is

$$H^{(-)} = -\frac{\Delta}{2m} - i\beta \vec{A}(t) \cdot \vec{\nabla}, \quad (2)$$

and the Hamiltonian for protons can be written as

$$H^{(+)} = -\frac{\Delta}{4M} + \frac{1}{2r}, \quad (3)$$

where we introduce the reduced mass $m = \frac{2M}{2M+1} \approx 1$ and $\beta = \frac{1+M}{M} \approx 1$ for the electron, and $\vec{A}(t)$ is the vector potential. The Hamiltonian of the electron-proton interaction can be written as

$$H_{EP} = -\frac{1}{|\vec{r}_1 + \vec{r}_2|} - \frac{1}{|\vec{r}_1 - \vec{r}_2|}. \quad (4)$$

B. t-SURFF for dissociative ionization

The t-SURFF method is applied here for the dissociative ionizations, which was successfully applied to the polyelectron molecules and to the double emission of the He atom [16,28–31]. In this section, we will follow a similar procedure as is done in Ref. [16].

According to the approximations of the t-SURFF method, beyond a sufficiently large t-SURFF radius $R_c^{(+/-)}$, the interactions of protons and electrons can be neglected, with the corresponding Hamiltonians being $H_V^{(+)} = -\frac{\Delta}{4M}$ for two protons and $H_V^{(-)} = -\frac{\Delta}{2m} - i\beta \vec{A}(t) \cdot \vec{\nabla}$ for the electron. The scattered states of the two protons, which satisfy $i\partial_t \chi_{\vec{k}_1}(\vec{r}_1) = H_V^{(+)} \chi_{\vec{k}_1}(\vec{r}_1)$, are

$$\chi_{\vec{k}_1}(\vec{r}_1) = \frac{1}{(2\pi)^{3/2}} \exp\left(-i \int_{t_0}^t \frac{k_1^2}{4M} d\tau\right) \exp(i\vec{k}_1 \cdot \vec{r}_1), \quad (5)$$

and those of the electron, which satisfies $i\partial_t \chi_{\vec{k}_2}(\vec{r}_2) = H_V^{(-)} \chi_{\vec{k}_2}(\vec{r}_2)$, are

$$\chi_{\vec{k}_2}(\vec{r}_2) = \frac{1}{(2\pi)^{3/2}} \exp\left(-i \int_{t_0}^t \frac{k_2^2}{2m} - i\beta \vec{A}(\tau) \cdot \vec{\nabla} d\tau\right)$$
$$\times \exp(i\vec{k}_2 \cdot \vec{r}_2), \quad (6)$$

where we assume the laser field starts at t_0 and $\vec{k}_{1/2}$ denote the momenta of the protons or the electron.
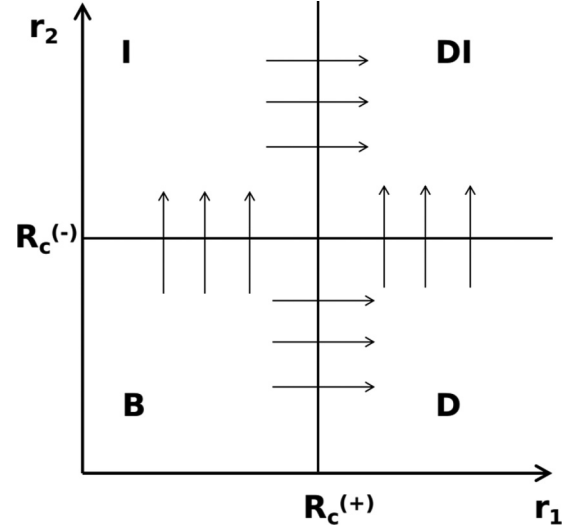

FIG. 1. The regions of dissociative ionization time propagation. The B stands for the bound region, and D for the dissociation region where the two protons are out of $R_c^{(+)}$ but the electron is not ionized and stays inside. I represents the ionization region where the electron is out-of-box $R_c^{(-)}$ but two protons are still inside $R_c^{(+)}$. DI stands for the dissociative ionization region where both the electron and the protons are out of $R_c^{(+/-)}$. $R_c^{(+/-)}$ are the t-SURFF radii for $r_1 = |\vec{r}_1|$ or $r_2 = |\vec{r}_2|$.

Based on the t-SURFF radius $R_c^{(+/-)}$, we may split the dissociative ionization into four regions, namely B, I, D, DI, shown in Fig. 1, where the bound region B preserves the full Hamiltonian in Eq. (1), D, I are time propagations by single particles with the Hamiltonians

$$H_D(\vec{r}_2, t) = H_V^{(-)}(\vec{r}_2, t) = -\frac{\Delta}{2m} - i\beta \vec{A}(t) \cdot \vec{\nabla} \quad (7)$$

and

$$H_I(\vec{r}_1, t) = -\frac{\Delta}{4M} + \frac{1}{2r_1}, \quad (8)$$

and DI is an integration process. The treatment was first introduced in the double ionization of helium in Ref. [15] and then applied in a 2D simulation of the H_2^+ ion in Ref. [19]. Without considering the low-energy free electrons that stay inside the box after time propagation, we may write

$$\psi_B(\vec{r}_1, \vec{r}_2, t) \approx 0, \quad r_1 \geqslant R_c^{(+)}, \quad \text{or } r_2 \geqslant R_c^{(-)},$$
$$\psi_D(\vec{r}_1, \vec{r}_2, t) \approx 0, \quad r_1 < R_c^{(+)}, \quad \text{or } r_2 \geqslant R_c^{(-)},$$
$$\psi_I(\vec{r}_1, \vec{r}_2, t) \approx 0, \quad r_1 \geqslant R_c^{(+)}, \quad \text{or } r_2 < R_c^{(-)},$$
$$\psi_{DI}(\vec{r}_1, \vec{r}_2, t) \approx 0, \quad r_1 < R_c^{(+)}, \quad \text{or } r_2 < R_c^{(-)}. \quad (9)$$

We assume that for a sufficiently long propagation time T, the scattering ansatz of the electron and protons disentangles. By introducing the step function

$$\Theta_{1/2}(R_c) = \begin{cases} 0, & r_{1/2} < R_c^{(+/-)}, \\ 1, & r_{1/2} \geqslant R_c^{(+/-)}, \end{cases} \quad (10)$$

the unbound spectra can be written as

$$P(\vec{k}_1, \vec{k}_2) = P(\phi_1, \theta_1, k_1, \phi_2, \theta_2, k_2) = |b(\vec{k}_1, \vec{k}_2, T)|^2. \quad (11)$$

$b(\vec{k}_1, \vec{k}_2, T)$ are the scattering amplitudes and can be written as

$$b(\vec{k}_1, \vec{k}_2, T) = \left\langle \chi_{\vec{k}_1} \otimes \chi_{\vec{k}_2} \middle| \Theta_1(R_c)\Theta_2(R_c) \middle| \psi(\vec{r}_1, \vec{r}_2, t) \right\rangle$$

$$= \int_{-\infty}^{T} [F(\vec{k}_1, \vec{k}_2, t) + \bar{F}(\vec{k}_1, \vec{k}_2, t)]dt, \quad (12)$$

with two sources written as

$$F(\vec{k}_1, \vec{k}_2, t) = \left\langle \chi_{\vec{k}_2}(\vec{r}_2, t) \middle| [H_V^{(-)}(\vec{r}_2, t), \Theta_2(R_c)] \middle| \varphi_{\vec{k}_1}(\vec{r}_2, t) \right\rangle \tag{13}$$

and

$$\bar{F}(\vec{k}_1, \vec{k}_2, t) = \left\langle \chi_{\vec{k}_1}(\vec{r}_1, t) \middle| [H_V^{(+)}(\vec{r}_1, t), \Theta_1(R_c)] \middle| \varphi_{\vec{k}_2}(\vec{r}_1, t) \right\rangle. \tag{14}$$

The single-particle wave functions $\varphi_{\vec{k}_1}(\vec{r}_2, t)$ and $\varphi_{\vec{k}_2}(\vec{r}_1, t)$ satisfy

$$i\frac{d}{dt}\varphi_{\vec{k}_1}(\vec{r}_2, t) = H_D(\vec{r}_2, t)\varphi_{\vec{k}_1}(\vec{r}_2, t) - C_{\vec{k}_1}(\vec{r}_2, t) \tag{15}$$

and

$$i\frac{d}{dt}\varphi_{\vec{k}_2}(\vec{r}_1, t) = H_I(\vec{r}_1, t)\varphi_{\vec{k}_2}(\vec{r}_1, t) - C_{\vec{k}_2}(\vec{r}_1, t). \tag{16}$$

The sources are the overlaps of the two-electron wave function and the Volkov solutions shown by

$$C_{\vec{k}_1}(\vec{r}_2, t) = \int d\vec{r}_1 \overline{\chi_{\vec{k}_1}(\vec{r}_1, t)} [H_V^{(+)}(\vec{r}_1, t), \Theta_1(R_c)] \psi(\vec{r}_1, \vec{r}_2, t) \tag{17}$$

and

$$C_{\vec{k}_2}(\vec{r}_1, t) = \int d\vec{r}_2 \overline{\chi_{\vec{k}_2}(\vec{r}_2, t)} [H_V^{(-)}(\vec{r}_2, t), \Theta_2(R_c)] \psi(\vec{r}_1, \vec{r}_2, t), \tag{18}$$

with initial values being 0, where $\overline{\cdots}$ means complex conjugate. The two t-SURFF radii could be set to equivalent $R_c^{(+)} = R_c^{(-)}$, because all Coulomb interactions are neglected when either the protons or electron are out of the t-SURFF radius. According to our previous research, the spectrum computation is independent of the R_c if all Coulomb terms are removed and the wave function is propagated long enough after the pulse [15,16]. The t-SURFF for the double emission of two particles was first introduced in Ref. [15]. The above derivations are very similar to what was reported in Ref. [16] for the double emission of helium, where the only differences are the constants before different operators, say, Δ, $\vec{\nabla}$, and $\frac{1}{r}$. Thus, detailed formulas are omitted here and the interested readers can refer to Refs. [15,16].

The computation for the photoelectron spectrum includes four steps, similar to the one used in Ref. [16], detailed as follows:

(1) Solve the full 6D TDSE with the Hamiltonian in the B region, given in Eq. (1), and write the time-dependent surface values in the disk.

(2) Evolve the single-particle wave packets in the D region by Eq. (13) with surface values given in the B region time propagation.

(3) Evolve the single-particle wave packets in the I region by Eq. (14) with the surface values given in the B region time propagation.

(4) Integrate the fluxes calculated from surface values written in the D and I regions' time propagation by Eq. (12).

III. NUMERICAL IMPLEMENTATIONS

The numerical methods here are similar to what was detailed in Refs. [16,18]. In fact, the code in this paper is developed based on the double-ionization framework of the tRecX code used in Refs. [16,18]. Thus, we will focus on the electron-proton interaction which was not mentioned before and only list relevant discretization methods in this paper.

A. Discretization and basis functions

The 6D wave function ψ is represented by the product of spherical harmonics for angular momentum and radial functions as

$$\psi(\vec{r}_1, \vec{r}_2, t) = \psi(r_1, \theta_1, \phi_1, r_2, \theta_2, \phi_2, t)$$

$$= \sum_{m_1, l_1, m_2, l_2} Y_{l_1}^{m_1}(\theta_1, \phi_1) Y_{l_2}^{m_2}(\theta_2, \phi_2)$$

$$\times R_{m_1, m_2, l_1, l_2}(r_1, r_2, t), \tag{19}$$

where $Y_{l_1}^{m_1}(\theta_1, \phi_1)$ and $Y_{l_2}^{m_2}(\theta_2, \phi_2)$ are the spherical harmonics of the two electrons and the radial function is represented by the finite-element discrete variable representation (FE-DVR) method as

$$R_{m_1, m_2, l_1, l_2}(r_1, r_2, t) = \sum_{n_1, n_2} R_{m_1, m_2, l_1, l_2}^{n_1, n_2}(r_1, r_2, t),$$

$$R_{m_1, m_2, l_1, l_2}^{n_1, n_2}(r_1, r_2, t) = \sum_{p_1, p_2} f_{p_1}^{(n_1)}(r_1) f_{p_2}^{(n_2)}(r_2) \frac{1}{r_1 r_2}$$

$$\times c_{n_1, n_2, p_1, p_2}^{m_1, m_2, l_1, l_2}(t), \tag{20}$$

where $f_{p_{1/2}}^{(n_{1/2})}(r_{1/2})$ are $p_{1/2}$th basis functions on the $n_{1/2}$th element, and the time dependencies of the three particles are included in the radial functions and coefficients $c_{n_1, n_2, p_1, p_2}^{m_1, m_2, l_1, l_2}(t)$, as is used in Refs. [15,16]. The infinite-range exterior complex scaling (irECS) method is utilized as an absorber [33]. The t-SURFF expression for computing the spectra of such a discretization can be found in Ref. [16].

B. Electron-proton interaction

The first part of the electron-proton interaction can be written in a multipole expansion as

$$\frac{1}{|\vec{r}_1 - \vec{r}_2|} = \frac{1}{\sqrt{r_1^2 + r_2^2 - 2r_1 r_2 \cos\gamma}}$$

$$= \frac{1}{r_>} \frac{1}{\sqrt{1 + h^2 - 2h\cos\gamma}} = \sum_{l=0}^{\infty} \frac{h^l}{r_>} P_l(\cos\gamma), \tag{21}$$

where $r_> = \max(r_1, r_2)$, $r_< = \min(r_1, r_2)$, $h = \frac{r_<}{r_>}$, γ is the angle between $\vec{r}_1, \vec{r}_2$, and $P_l(\cos\gamma)$ are Legendre polynomials. Similarly, we have

$$\frac{1}{|\vec{r}_1 + \vec{r}_2|} = \frac{1}{r_>} \frac{1}{\sqrt{1 + h^2 + 2h\cos\gamma}} = \sum_{l=0}^{\infty} (-1)^l \frac{h^l}{r_>} P_l(\cos\gamma), \tag{22}$$

and the summation goes as

$$\frac{1}{|\vec{r}_1 + \vec{r}_2|} + \frac{1}{|\vec{r}_1 - \vec{r}_2|} = 2 \sum_{l=0}^{\infty} \frac{h^l}{r_>} P_l(\cos\gamma) \quad l \bmod 2 = 0,$$
(23)

where $l \bmod 2 = 0$ means l is even. With the Legendre polynomials expanded by spherical harmonics $Y_l^m(\theta_2, \phi_2)$ and $Y_l^{m*}(\theta_1, \phi_1)$, we have

$$H_{EP} = -2 \sum_{l=0}^{\infty} \sum_{m=-l}^{l} \frac{4\pi}{2l+1} \frac{r_<^l}{r_>^{l+1}} Y_l^m(\theta_2, \phi_2) Y_l^{m*}(\theta_1, \phi_1)$$

$$l \bmod 2 = 0.$$
(24)

The matrix elements of electron-proton interaction are

$$\langle \psi_{m_1', m_2', l_1', l_2'}^{(n_1', n_2')}| -\frac{1}{|\vec{r}_1 - \vec{r}_2|} - \frac{1}{|\vec{r}_1 + \vec{r}_2|} |\psi_{m_1, m_2, l_1, l_2}^{(n_1, n_2)}\rangle$$

$$= -2 \sum_{\lambda\mu} \frac{4\pi}{2\lambda+1} \langle Y_{l_1'}^{m_1'} Y_\lambda^\mu | Y_{l_1}^{m_1}\rangle \langle Y_{l_2'}^{m_2'} | Y_\lambda^\mu Y_{l_2}^{m_2}\rangle$$

$$\times \langle R_{m_1', m_2', l_1', l_2'}^{n_1', n_2'} | \frac{r_<^\lambda}{r_>^{\lambda+1}} | R_{m_1, m_2, l_1, l_2}^{n_1, n_2}\rangle, \quad \lambda \bmod 2 = 0, \quad (25)$$

which could be obtained by dropping the odd λ terms and multiplying the even λ terms by -2 in the standard multipole expansion for electron-electron interactions from Ref. [16] as

$$\langle \psi_{m_1' m_2' l_1' l_2'}^{(n_1' n_2')} | \frac{1}{|\vec{r}_1 - \vec{r}_2|} | \psi_{m_1, m_2, l_1, l_2}^{(n_1 n_2)}\rangle$$

$$= \sum_{\lambda\mu} \frac{4\pi}{2\lambda+1} \langle Y_{l_1'}^{m_1'} Y_\lambda^\mu | Y_{l_1}^{m_1}\rangle \langle Y_{l_2'}^{m_2'} | Y_\lambda^\mu Y_{l_2}^{m_2}\rangle$$

$$\times \langle R_{m_1', m_2', l_1', l_2'}^{n_1' n_2'} | \frac{r_<^\lambda}{r_>^{\lambda+1}} | R_{m_1, l_1, m_2, l_2}^{n_1 n_2}\rangle.$$
(26)

Here,

$$\psi_{m_1, m_2, l_1, l_2}^{(n_1, n_2)} = Y_{l_1}^{m_1}(\theta_1, \phi_1) Y_{l_1}^{m_1}(\theta_2, \phi_2) R_{m_1, m_2, l_1, l_2}^{n_1, n_2}(r_1, r_2, t).$$
(27)

Therein, the matrix for the electron-proton interaction could be obtained by the numerical recipes used in Refs. [16,34] with limited changes. Numerically, we find λ does not need to go to infinity and a maximum value of 8 already suffices for our simulations.

IV. NUMERICAL RESULTS

A numerical convergence study shows, unlike the 6D double emission of He, where $m_{1/2} = 0$, $0 \leqslant l_{1/2} \leqslant 2$ already gives a convergent ground eigenenergy [16]; here, the angular quantum number $0 \leqslant m_{1/2} \leqslant 2$ and $0 \leqslant l_{1/2} \leqslant 8$ start to give convergent calculations, due to the lower symmetric property of the H_2^+ ion. The $R_c^{(+)} = R_c^{(-)} = 12.5$ atomic units is chosen for the computation, as we find $R_c^{(-)}$ does not change the quality of the spectrum but introduces a longer propagation time for low-energy particles to fly out. $R_c^{(+)} = 12.5$ atomic units gives the internuclear distance $R = 25$ atomic units as used in Ref. [19]. According to the convergence study in Appendix B, $R_c^{(+)} = R_c^{(-)} = 12.5$ atomic units gives a JES with an error below 10%. $R_c^{(-)} = 12.5$ atomic units is much larger than the quiver radius of an electron in a 400-nm,

8.3×10^{13} W/cm^2 laser pulse. Reference [35] shows the Coulomb explosion at large distances contributes to the low-energy fragments of protons, which are highly correlated to the resonances between two H_2^+ eigenstates. Thus we need a large simulation box to include all possible eigenenergies. In Ref. [35], the maximum internuclear distance for the low-energy fragments is 11 atomic units. The molecular eigenenergies are nearly invariant with an internuclear distance far below our $2R_c^{(+)} = 25$ atomic units here. Any potential dynamic dissociation quenching effect (DDQ) is also included in the B region because the H_2^+ is in a dissociative limit with an internuclear distance over 12 atomic units [36]. The wave function is propagated long enough after the pulse to include the unbound states with low kinetic energies.

If the kinetic energy of protons is included, the field-free ground-energy value is $E_0 = -0.592$ atomic units and the internuclear distance is 2.05 atomic units. With the kinetic energy of protons excluded, the ground eigenenergy is -0.597 atomic units, three digits exact to the ground energy from quantum chemistry calculations in Ref. [37], where the internuclear distance is fixed. The internuclear distance is 1.997 atomic units, three digits exact to that from the precise computations in Ref. [38].

A. Laser pulses

The dipole field of a laser pulse with a peak intensity $I = \mathcal{E}_0^2$ (atomic units) and linear polarization in the z direction is defined as $\mathcal{E}_z(t) = -\partial_t A_z(t)$, phase $\phi_{CEP} = 0$ with

$$A_z(t) = \frac{\mathcal{E}_0}{\omega} a(t) \sin(\omega t + \phi_{CEP}).$$
(28)

A pulse with $\lambda = 400$ nm is given with intensities 8.3×10^{13} W/cm^2 close to the 2D computation in Ref. [19] and 5.9×10^{13} W/cm^2 close to the experimental conditions in Ref. [12]. We choose $a(t) = [\cos(t/T)]^8$ as a realistic envelope. Pulse durations are specified as full width at half maximum FWHM = 5 opt. cyc. (optical cycle) with regard to intensity. To compare with the published results, a 400-nm, sin^2 envelope laser pulse at 8.8×10^{13} W/cm^2 from Ref. [19] and a 791-nm, cos^8 laser pulse at 7.7×10^{13} W/cm^2 used in Ref. [39] are also applied.

B. Joint energy spectra

The JES of the two dissociative protons and the electron is obtained by integrating Eq. (11) over angular coordinates as

$$\sigma(E_N, E_e) = \int d\phi_1 \int d\phi_2 \int d\theta_1 \sin\theta_1 \int d\theta_2 \sin\theta_2$$

$$\times P(\phi_1, \theta_1, \sqrt{4ME_N}, \phi_2, \theta_2, \sqrt{2mE_e}), \quad (29)$$

where E_N, E_e are kinetic energies of *two protons* and an electron, respectively. $\sigma(E_N, E_e)$ is presented in Figs. 2(a) and 2(b). The tilt lines with formula $E_N + E_e = N\omega + E_0 - U_p$ with ponderomotive energy $U_p = \frac{A_0^2}{4m}$ specify the energy sharing of N photons for both the computations from 8.3×10^{13} W/cm^2 and 5.9×10^{13} W/cm^2, indicating correlated emissions of the electron and protons, which are also observed in the 2D computations [19,20]. The yields are intense around the nuclear KER from 2 to 4 eV in the cos^8 envelope
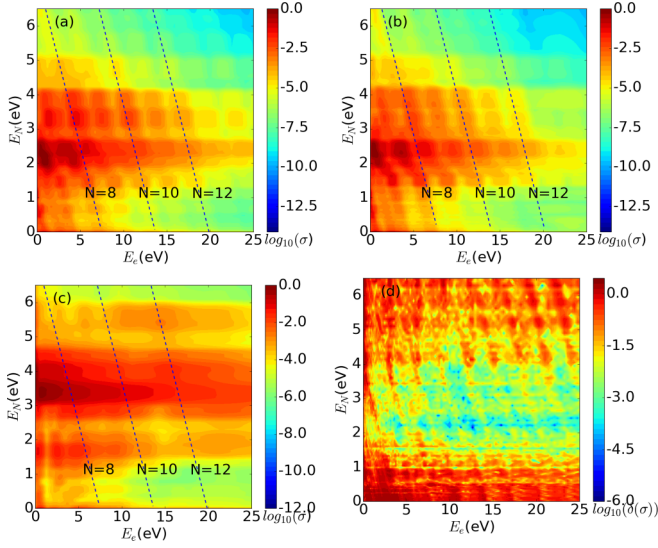
FIG. 2. Log-scale JES $\log_{10} \sigma(E_N, E_e)$ represented by the total energy of two protons E_N and that of an electron E_e. Linearly polarized, 400 nm, with (a) $\cos^8$ envelope with FWHM = 5 opt. cyc. at 8.3×10^{13} W/cm^2 and (b) $\cos^8$ envelope with FWHM = 5 opt. cyc. pulses at 5.9×10^{13} W/cm^2 is applied to the H$_2^+$ ion. The dashed lines represent the energy sharing between the protons and electron with formula $E_N + E_e = N\omega + E_0 - U_p$, where ω is the photon energy. (c) JES from Coulomb explosion simulation from the ground eigenstate of the H$_2^+$ ion. (d) Log-scale error $\log[\delta(\sigma)]$ of two spectra from $\cos^8$ envelope laser pulse at 8.3×10^{13} W/cm^2 with and without the contribution from $D \to DI$ [from Eq. (13)] by $\delta(\sigma) = 2 \frac{|\sigma'(E_N, E_e) - \sigma(E_N, E_e)|}{|\sigma'(E_N, E_e) + \sigma(E_N, E_e)|}$. $\sigma(E_N, E_e)$ of (a) and (b) are normalized with dividing by the maximum value.

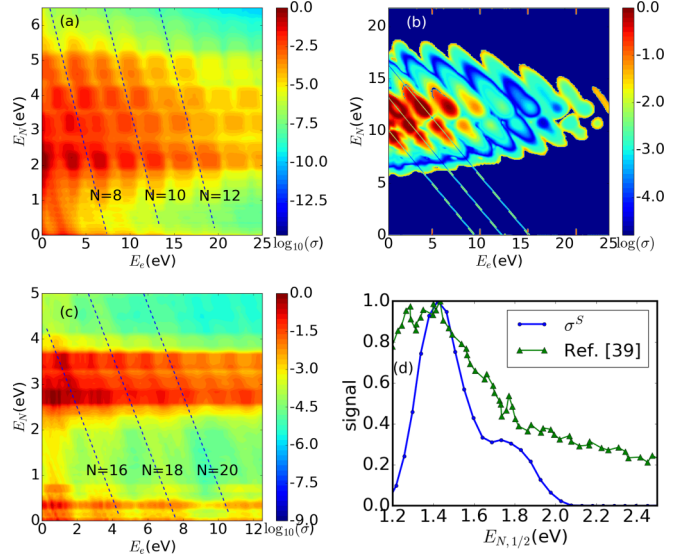
FIG. 3. Log-scale JES $\log_{10} \sigma(E_N, E_e)$ represented by the total energy of two protons E_N and that of an electron E_e. JES of H$_2^+$ in a linearly polarized, 400-nm laser pulse at 8.8×10^{13} W/cm^2 as is used in Ref. [19] by (a) 6D computation compared to (b) the normalized 2D data from Ref. [19], and (c) in a linearly polarized, 791-nm laser pulse at 7.7×10^{13} W/cm^2 as used in Ref. [39]. (d) Blue dots: The normalized single JES is created from $\sigma^S(E_{N,1/2}) = \int \sigma(2E_{N,1/2}, E_e)\sqrt{E_e}dE_e$, where $E_{N,1/2}$ depicts the kinetic energy of a proton. Green triangles: The normalized signals extracted from Ref. [39] with respect to the kinetic energy of a proton.

pulse, consistent with the experimental values reported in Refs. [12,13]. The peak of JES for dissociative ionization is for a lower nuclear KER than that (3–4 eV) from a Coulomb explosion from the ground eigenstate of the H$_2^+$ ion, whose property is also close to experimental observables [39]. The Coulomb explosion JES is obtained with the same method as dissociative ionization except that H_{EP} is removed from the B region Hamiltonian as $H_B^{(CS)} = H^{(+)} \otimes \mathbb{1} + \mathbb{1} \otimes H^{(-)}$, but the initial state is still obtained from the Hamiltonian H_B in Eq. (1). We find that the contribution from time propagation in the subregion $D \to DI$ [see Eq. (13)] is small, as the numerical error of JES $\delta(\sigma)$ of σ computed from $I \to DI$, and σ' computed from two subregions ($I \to DI$ and $D \to DI$) is always below 1% of the main contribution of the JES ($2 < E_N < 4$ eV); see Fig. 2(d). This numerical property is also observed in two-dimensional (2D) simulations [19]. This is because the electrons are much faster than protons and the H$_2^+$ ion tends to release first.

Here, we compare our computations with the published results. First, the JES with a 400-nm, $\sin^2$ envelope laser pulse at 8.8×10^{13} W/cm^2 as used in the 2D simulations in Ref. [19] is computed [see Fig. 3(a), compared to the results from 2D simulations in Fig. 3(b)]. One clearly sees the JES is most considerable with a nuclear KER around 2–4 eV in our computation but is with nuclear KER above 10 eV in the 2D simulation. We also attach the JES with a linearly polarized, 791-nm laser pulse at 7.7×10^{13} W/cm^2 as used in Ref. [39],

where JES is most considerable with a nuclear KER around 3 eV. For the 791-nm computation, $R_c^{(-)} = 15$ atomic units is applied, which is slightly above the quiver radius of the electron. For a direct comparison, we integrate the JES over the electron KER and obtain the photoelectron spectrum with respect to the nuclear KER in Fig. 3(d), where the experimental data from Ref. [39] are also attached. The peak of the spectrum around 1.42 eV in our computation is in good agreement with the experimental data, and the position of a minor peak around 1.7 eV in our computation also matches the experimental observation. The observation that JES is most considerable with a nuclear KER around 2–4 eV can also be found in the Coulomb explosion computation shown in Fig. 2(c). In the experiments reported by other groups, the distribution of emitted protons peaks at nuclear KER = 4 eV for a 780-nm laser pulse at 6×10^{14} W/cm^2 [11], and Refs. [12,13] reported that the largest possible nuclear KER is around 3 eV for two protons with 400-nm laser pulses. These observables at different experimental conditions show that the largest possible nuclear KERs are around 2–4 eV, which are close to our computations but far from the computations in the 2D simulations [14,19]. This seems to contradict to energy conservation for classical particles that the Coulomb explosion most probably starts at an internuclear distance $R = 2r_1 = 2$ atomic units, which gives a nuclear KER of 0.5 atomic units. We now consider the wave-packet dispersion in different coordinates. For a 1D simulation on protons with a symmetric Gaussian wave packet, the center of the wave packet moves with the velocity of the classical particle, thus

the largest possible nuclear KER is 0.5 atomic units, which is close to the results in the existing 2D simulations [14,19]. In a 3D simulation on protons, the wave packet keeps expanding perpendicular to the polarization direction and is not symmetric on the r_1 axis (see Fig. 6). A numerical study with a simple unphysical toy model in Appendix C shows that for the Coulomb explosion in spherical coordinates, the most probable nuclear KER can be shifted to 1/4–1/3 of the total kinetic energy and the right half curve of the integrated JES is less steep [see Fig. 6(a)]. The longer tail in the higher nuclear KER for an integrated JES of H_2^+ is also observed both in experiments and our computation, but not in the 1D simulation on protons [see Figs. 3(d) and 7]. Thus, the reason why we get a much lower most probable nuclear KER is that we give a 3D simulation of the wave-function dispersion of protons, which may not be correctly approximated with the 1D treatment in 2D simulations. The existing 2D simulations for the dissociative ionization put corrections to the electron-proton interaction with a softening parameter to give the correct ground energy of electrons in H_2^+ [14,19]. However, the pure Coulomb repulsion of the two protons $1/R$ (R is the internuclear distance) is included without a softening parameter. We would like to point out that, for the 2D simulation, for consistency of the correction of the Coulomb interaction of the electron, the Coulomb repulsion term of the two protons may also need a softening parameter, whose value needs further investigations.

C. Angular distribution

The projected energy distribution on the azimuth angle of the electron and the protons is calculated by integrating the 6D scattering amplitudes as

$$p_N(\theta_1, E_1) = \int d\vec{k}_2 \int d\phi_1 |b(\vec{k}_1, \vec{k}_2, T)|^2,$$
$$\vec{k}_1 = [\phi_1, \theta_1, \sqrt{8ME_1}]^T, \tag{30}$$

for protons, and

$$p_e(\theta_2, E_2) = \int d\vec{k}_1 \int d\phi_2 |b(\vec{k}_1, \vec{k}_2, T)|^2,$$
$$\vec{k}_2 = [\phi_2, \theta_2, \sqrt{2mE_2}]^T, \tag{31}$$

for an electron, where E_1 and E_2 are kinetic energies for *an individual* proton and electron.

As is observed in Fig. 4, the probability distributions of electron and protons reach the highest value in the polarization direction, which is consistent with the experimental observations for linearly polarized laser pulses [11,13]. The probability of the dissociative protons is most considerable with $1 \leqslant E_1 \leqslant 2$ eV, higher than the $E_1 < 1$ eV for dissociative channels reported in Refs. [11,39], but in the range of their Coulomb explosion channel, where the laser wavelength is 800 nm. For a higher intensity 8.3×10^{13} W/cm² , the angular distribution of released protons and the electron extends more in the polarization direction. For the distribution of protons, tiny yields around 3 eV in the radial coordinates indicate the Coulomb explosion channel, close to what is observed in experiments, however, for different laser pulses [39].
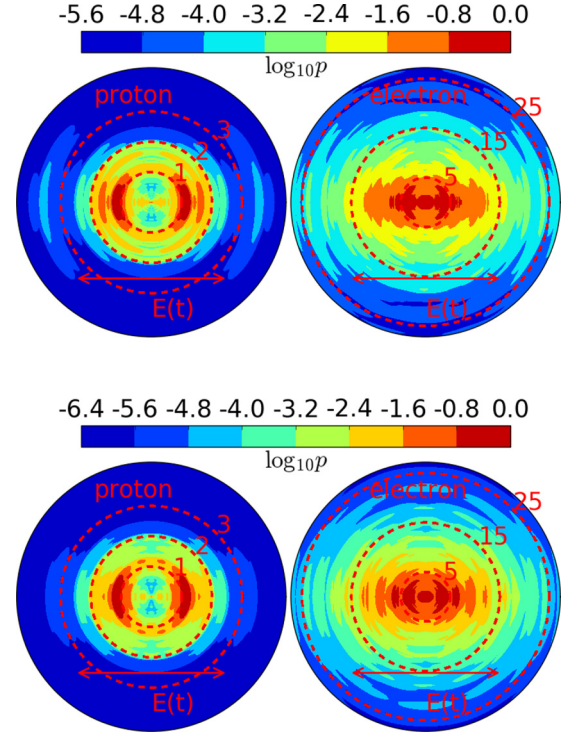

FIG. 4. The log-scale probability distribution of (left column) protons by $\log_{10} p_N(\theta_1, E_1)$ and (right column) protons by $\log_{10} p_e(\theta_2, E_2)$, $\theta_{1,2} \in [0, \pi]$. The plot is symmetrized by $p_N(2\pi - \theta_1, E_1) = p_N(2\pi - \theta_1, E_1)$ and $p_e(2\pi - \theta_2, E_2) = p_e(2\pi - \theta_2, E_2)$. The upper row is computed from a laser pulse at intensity 8.3×10^{13} W/cm² and the lower row represents 5.9×10^{13} W/cm². The values of the radial coordinates $E_{1/2}$ are represented in eV. The polarization direction is along the horizontal axis and the direction of the electric field is labeled in each subfigure with an arrow and a label "$E(t)$." The values are all normalized with dividing by the maximum value.

V. CONCLUSION AND DISCUSSIONS

We simulate the dissociative ionization of the H_2^+ ion in full dimensionality and have obtained the same ground eigenenergy as that from the quantum chemistry computations. Using t-SURFF methods, we obtained the JES where energy sharing is observed, which indicates a correlation between the electron and protons. The JES peaked at E_N from 2 to 4 eV, which is different from previous 2D simulations, but is consistent with the experimental data. The difference indicates that in the dissociative ionization of H_2^+, the protons should be treated quantum mechanically in full dimensionality by simulating the 3D wave-function evolution, where the expansion of the wave packets perpendicular to the radial direction may need to be taken into consideration. The projected energy distribution on angles shows that the electron and protons tend to dissociate in the direction of polarization of the laser pulse.

The simulation of the single emission spectrum showing dissociation channels, is, however, not yet possible. The difficulty lies mainly in constructing the internuclear-distance-dependent electronic ansatz of H with a given ionic state in a single emission TDSE on $\vec{r}_1$, which might be solved by reading the energy surfaces from quantum chemistry calculations or another tRecX calculation. This is left for future work.

APPENDIX A: COORDINATE TRANSFORMATION

We use subindices a, b, and e to present the two protons and the electron of an arbitrary coordinate. The subindices 0, 1, and 2 represent the center of the two protons, the relative position of a proton to the center, and the electron in our transformed coordinate, respectively. Suppose the coordinates of the two protons and the electron are initially represented by vectors $\vec{x}_a$, $\vec{x}_b$, and $\vec{x}_e$ of an arbitrary origin, respectively. The new coordinates $\vec{r}_1$ and $\vec{r}_2$ satisfy

$$\vec{r}_0 = \frac{\vec{x}_a + \vec{x}_b}{2}, \quad \vec{r}_1 = \frac{\vec{x}_a - \vec{x}_b}{2}, \quad \vec{r}_2 = \vec{x}_e - \frac{\vec{x}_a + \vec{x}_b}{2},$$
$$\text{(A1)}$$

where $\vec{r}_0$ is the coordinate of the center of the two protons. The Laplacians of the two protons ∇_a^2, ∇_b^2 and the electron ∇_e^2 are

$$\nabla_a^2 = \frac{\nabla_0^2}{4} + \frac{\nabla_1^2}{4} + \frac{\nabla_2^2}{4} + \frac{\vec{\nabla}_0 \cdot \vec{\nabla}_1}{2} - \frac{\vec{\nabla}_1 \cdot \vec{\nabla}_2}{2} - \frac{\vec{\nabla}_2 \cdot \vec{\nabla}_0}{2},$$

$$\nabla_b^2 = \frac{\nabla_0^2}{4} + \frac{\nabla_1^2}{4} + \frac{\nabla_2^2}{4} - \frac{\vec{\nabla}_0 \cdot \vec{\nabla}_1}{2} + \frac{\vec{\nabla}_1 \cdot \vec{\nabla}_2}{2} - \frac{\vec{\nabla}_2 \cdot \vec{\nabla}_0}{2},$$

$$\nabla_e^2 = \nabla_2^2. \qquad\qquad\qquad\qquad\qquad\qquad\qquad\qquad \text{(A2)}$$

Thus the kinetic energy of the system can be represented by

$$-\frac{1}{2}\left(\frac{\nabla_a^2}{M} + \frac{\nabla_b^2}{M} + \frac{\nabla_e^2}{1}\right)$$

$$= -\frac{\nabla_0^2}{4M} - \frac{\nabla_1^2}{4M} - \frac{\nabla_2^2}{4M} + \frac{\vec{\nabla}_2 \cdot \vec{\nabla}_0}{M} + \frac{\nabla_2^2}{2}$$

$$\approx -\frac{\nabla_1^2}{4M} - \frac{\nabla_2^2}{2m}, \qquad\qquad\qquad\qquad \text{(A3)}$$
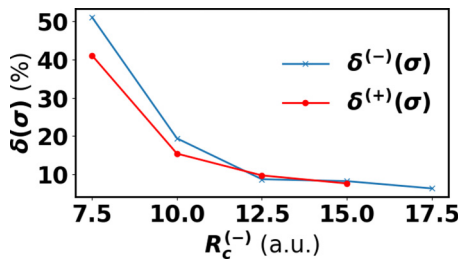

FIG. 5. The (blue crosses) error $\delta^{(+)}(\sigma)$ for $R_c^{(+)}$ by Eq. (B1) with fixed $R_c^{(-)} = 12.5$ atomic units and (red dots) error $\delta^{(-)}(\sigma)$ for computations for $R_c^{(-)}$ with fixed $R_c^{(+)} = 12.5$ atomic units. A 400-nm laser pulse at 8.8×10^{13} W/cm^2 is applied. For details of the laser pulse, refer to Sec. IV A. The parameters for angular momenta are $L_{\max} = 7$, $M_{\max} = 5$.
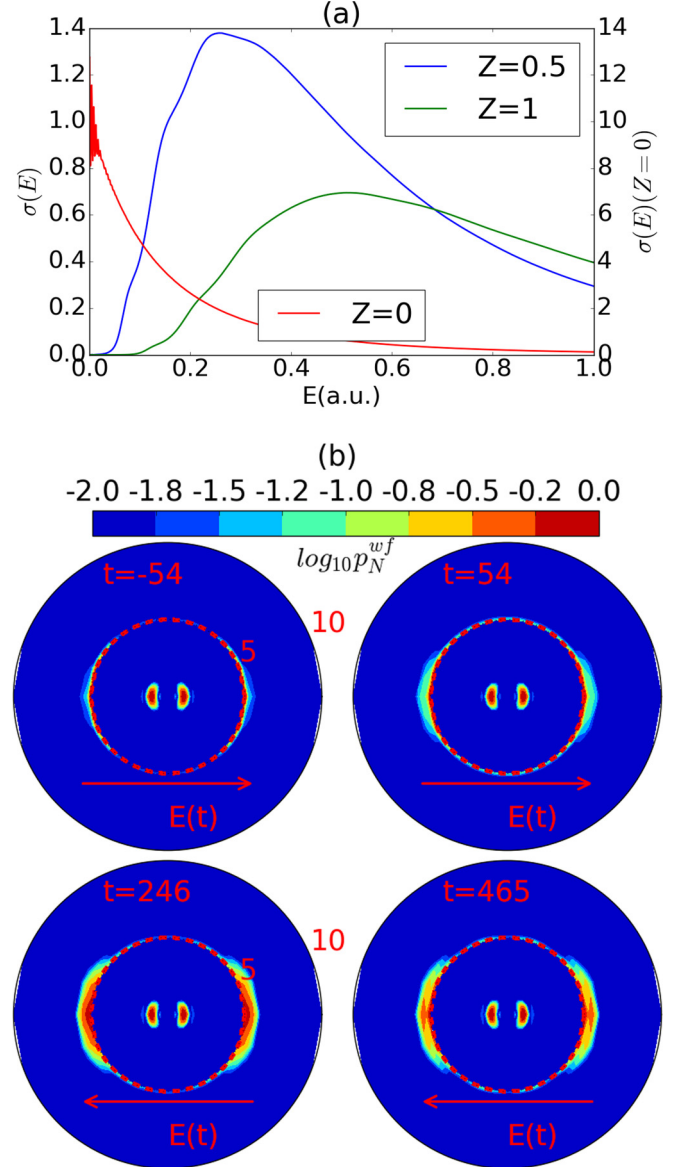

FIG. 6. (a) The energy spectrum $\sigma(E) = \int d\theta \int d\phi k |b(\vec{k}, T)|^2$, $E = \frac{k^2}{2}$, where $b(\vec{k}, T)$ are the single electron scattering amplitudes. The spectrum is computed by advancing a hydrogen electronic ground state in the Coulomb potential $+\frac{Z}{r}$. $Z = 0$ means no external Coulomb potential. The kinetic energy is computed by $\int_0^\infty \sigma(E)\sqrt{E}dE = Z + 0.5$ atomic units, consistent with energy conservation. (b) The log-scale probability distribution of protons is computed by $\log_{10} p_N^{\mathrm{wf}}(\phi_1, \theta_1, r_1, 0, 5, t)$, $r_1 \in [0, 5]$ of the inner shell and $\log_{10} p_N^{\mathrm{wf}}(\phi_1, \theta_1, r_1, 5, 10, t)$, $r_1 \in [5, 10]$ of the outer shell. $|E_z(t)|$ is considerable and reaches a local maximum when t $= -54$, 54, and 246 atomic units, which are also depicted in the figures. When $t = 465$ atomic units, $|E_z(t)|$ is very small. The whole space is split into two regions by the red, dashed circle, and the signals of each region are normalized independently. The polarization direction is along the horizontal axis and the direction of the electric field is labeled at each subfigure with an arrow and a label "$E(t)$." The absolute value of the outer shell is several orders smaller than the inner shell.

where $m = \frac{2M}{1+2M}$, and "$\approx$" means the motion of the $\vec{r}_0$ is neglected. The interaction of the two protons with the laser pulse can be written as

$$\frac{i}{M}\vec{A} \cdot (\vec{\nabla}_a + \vec{\nabla}_b) = i\vec{A} \cdot \frac{1}{M}(\vec{\nabla}_0 - \vec{\nabla}_2) \approx -\frac{i}{M}\vec{A} \cdot \vec{\nabla}_2, \quad (A4)$$

with which the total interaction with the laser field can be written as

$$-i\vec{A} \cdot \left(\vec{\nabla}_2 + \frac{1}{M}\vec{\nabla}_2\right) = -i\beta\vec{A} \cdot \vec{\nabla}_2, \quad (A5)$$

where $\beta = \frac{M+1}{M}$.

APPENDIX B: CONVERGENCE STUDY

The errors are computed by the difference of JES from two subsequent calculations $\sigma(E_N, E_e)$ and $\sigma'(E_N, E_e)$ with respect to $R_c^{(+)}$ and $R_c^{(-)}$,

$$\delta(\sigma) = \max_{E_N, E_e} 2\frac{|\sigma(E_N, E_e) - \sigma'(E_N, E_e)|}{|\sigma(E_N, E_e) + \sigma'(E_N, E_e)|}, \quad (B1)$$

as used previously in Fig. 2(c). As depicted in Fig. 5, the JES is converged at $R_c^{(+)} = R_c^{(-)} = 12.5$ atomic units with an error below 10%.

APPENDIX C: COULOMB EXPLOSION WITH DISPERSION OF WAVE PACKETS

Here, we illustrate the dispersion of the wave function with r in spherical coordinates by a simple but unphysical model: the Coulomb explosion of a hydrogen atom. It starts with the ground eigenstate of a hydrogen atom with an electronic wave function $\psi_0(\vec{r}) = \psi_0(r) = \frac{1}{\sqrt{\pi}}\exp(-r)$. The initial kinetic energy of the electron is 0.5 atomic units and the potential energy is -1 atomic units. Then, the charge of the nucleus suddenly changes from $+1$ to -1 and the kinetic energy remains the same, but the Coulomb potential reverses its sign. Thus the system explodes and the electron finally becomes a free particle. In what follows, we will discuss the largest possible kinetic energy of the free electron.
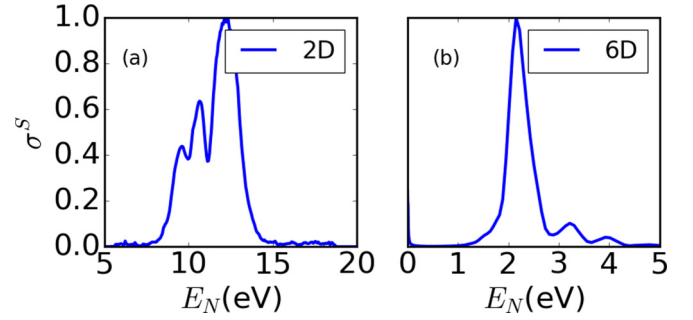

FIG. 7. The normalized single JES is created from (a) 2D and (b) 6D $\sigma^S(E_N) = \int \sigma(2E_N, E_e)\sqrt{E_e}dE_e$, where E_N depicts the kinetic energy of a proton. A laser pulse used in Ref. [19] is applied here. The 2D data are taken from Ref. [19].

In classical mechanics, the largest possible kinetic energy is 1.5 atomic units because of energy conservation. However, our quantum simulation by t-SURFF gives a value around 0.5 atomic units [see Fig. 6(a)]. We can also see that the distribution of the spectrum has long tails to the high-energy region. The integration of $\sigma(E)$ gives a total energy of 1.5 atomic units, which is consistent with energy conservation [see Fig. 6(a)].

The numerical simulations show the nuclear wave packets also expand in space during the time propagation [see Fig. 6(b)], where the probability distribution of the protons over time is computed by

$$p_N^{\text{wf}}(\phi_1, \theta_1, r_1, R_0, R_1, t)$$
$$= \int d\phi_2 \int \sin\theta_2 d\theta_2 \int_{R_0}^{R_1} r_2^2 dr_2 |\psi(\vec{r}_1, \vec{r}_2, t)|^2. \quad (C1)$$

We split the radial coordinates into the inner region $r_1, r_2 \in [R_0, R_1] = [0, 5]$ and outer region $r_1, r_2 \in [R_0, R_1] = [5, 10]$, and the yields of both regions are normalized with diving by the maximum probability of the region. Thus we attribute the difference of the most possible nuclear KER in JES to the 3D wave-function dispersion and expansion, which were not included in previous simulations. For simulations on dissociative ionization of H_2^+, the difference of dispersion of proton wave packets between 6D (3D for protons) and 2D (1D for protons) simulations could also be observed with the normalized single JES in Fig. 7.

[1] P. H. Bucksbaum, A. Zavriyev, H. G. Muller, and D. W. Schumacher, Phys. Rev. Lett. **64**, 1883 (1990).

[2] T. Zuo and A. D. Bandrauk, Phys. Rev. A **52**, R2511 (1995).

[3] G. Yao and S.-I. Chu, Phys. Rev. A **48**, 485 (1993).

[4] A. Giusti-Suzor, F. H. Mies, L. F. DiMauro, E. Charron, and B. Yang, J. Phys. B: At., Mol. Opt. Phys. **28**, 309 (1995).

[5] G. Jolicard and O. Atabek, Phys. Rev. A **46**, 5845 (1992).

[6] T. Zuo, S. Chelkowski, and A. D. Bandrauk, Phys. Rev. A **48**, 3837 (1993).

[7] B. D. Esry, A. M. Sayler, P. Q. Wang, K. D. Carnes, and I. Ben-Itzhak, Phys. Rev. Lett. **97**, 013003 (2006).

[8] J. H. Posthumus, Rep. Prog. Phys. **67**, 623 (2004).

[9] A. Giusti-Suzor, X. He, O. Atabek, and F. H. Mies, Phys. Rev. Lett. **64**, 515 (1990).

[10] M. Odenweller, N. Takemoto, A. Vredenborg, K. Cole, K. Pahl, J. Titze, L. P. H. Schmidt, T. Jahnke, R. Dörner, and A. Becker, Phys. Rev. Lett. **107**, 143004 (2011).

[11] M. Odenweller, J. Lower, K. Pahl, M. Schütt, J. Wu, K. Cole, A. Vredenborg, L. P. Schmidt, N. Neumann, J. Titze, T. Jahnke, M. Meckel, M. Kunitski, T. Havermeier, S. Voss, M. Schöffler, H. Sann, J. Voigtsberger, H. Schmidt-Böcking, and R. Dörner, Phys. Rev. A **89**, 013424 (2014).

[12] J. Wu, M. Kunitski, M. Pitzer, F. Trinter, L. P. H. Schmidt, T. Jahnke, M. Magrakvelidze, C. B. Madsen, L. B. Madsen, U. Thumm, and R. Dörner, Phys. Rev. Lett. **111**, 023002 (2013).

[13] X. Gong, P. He, Q. Song, Q. Ji, K. Lin, W. Zhang, P. Lu, H. Pan, J. Ding, H. Zeng, F. He, and J. Wu, Optica **3**, 643 (2016).

[14] C. B. Madsen, F. Anis, L. B. Madsen, and B. D. Esry, Phys. Rev. Lett. **109**, 163003 (2012).

[15] A. Scrinzi, New J. Phys. **14**, 085008 (2012).

[16] A. Zielinski, V. P. Majety, and A. Scrinzi, Phys. Rev. A **93**, 023406 (2016).

[17] L. Tao and A. Scrinzi, New J. Phys. **14**, 013021 (2012).

[18] J. Zhu and A. Scrinzi, Phys. Rev. A **101**, 063407 (2020).

[19] L. Yue and L. B. Madsen, Phys. Rev. A **88**, 063420 (2013).

[20] L. Yue and L. B. Madsen, Phys. Rev. A **90**, 063408 (2014).

[21] G. L. V. Steeg, K. Bartschat, and I. Bray, J. Phys. B: At., Mol. Opt. Phys. **36**, 3325 (2003).

[22] W. Qu, Z. Chen, Z. Xu, and C. H. Keitel, Phys. Rev. A **65**, 013402 (2001).

[23] R. E. F. Silva, F. Catoire, P. Rivière, H. Bachau, and F. Martín, Phys. Rev. Lett. **110**, 113001 (2013).

[24] N. Takemoto and A. Becker, Phys. Rev. Lett. **105**, 203004 (2010).

[25] B. Feuerstein and U. Thumm, Phys. Rev. A **67**, 043405 (2003).

[26] K. C. Kulander, F. H. Mies, and K. J. Schafer, Phys. Rev. A **53**, 2562 (1996).

[27] V. P. Majety and A. Scrinzi, Phys. Rev. Lett. **115**, 103002 (2015).

[28] V. P. Majety, A. Zielinski, and A. Scrinzi, J. Phys. B **48**, 025601 (2015).

[29] V. Majety and A. Scrinzi, Photonics **2**, 93 (2015).

[30] V. P. Majety, A. Zielinski, and A. Scrinzi, New J. Phys. **17**, 63002 (2015).

[31] V. P. Majety and A. Scrinzi, J. Phys. B **48**, 245603 (2015).

[32] J. R. Hiskes, Phys. Rev. **122**, 1207 (1961).

[33] A. Scrinzi, Phys. Rev. A **81**, 053845 (2010).

[34] C. W. McCurdy, M. Baertschy, and T. N. Rescigno, J. Phys. B **37**, R137 (2004).

[35] S. Chelkowski, T. Zuo, O. Atabek, and A. D. Bandrauk, Phys. Rev. A **52**, 2977 (1995).

[36] F. Châteauneuf, T. T. Nguyen-Dang, N. Ouellet, and O. Atabek, J. Chem. Phys. **108**, 3974 (1998).

[37] D. Bressanini, M. Mella, and G. Morosi, Chem. Phys. Lett. **272**, 370 (1997).

[38] L. J. Schaad and W. V. Hicks, J. Chem. Phys. **53**, 851 (1970).

[39] D. Pavičić, A. Kiess, T. W. Hänsch, and H. Figger, Phys. Rev. Lett. **94**, 163002 (2005).